Exploring the properties of the left angular gyrus using TMS-evoked potentials

Dominika Sulcova[a, 1], Yasmine Salman[a], Adrian Ivanoiu[a,b], André Mouraux[a]

a Institute of Neuroscience (IoNS), Université catholique de Louvain, 1200 Brussels, Belgium

b Cliniques Universitaires Saint-Luc, 1200 Brussels, Belgium

1 corresponding author

Contact information to the corresponding author:

dominika.sulcova@uclouvain.be; +32 484 38 54 33

ORCID identification:

D. Sulcova – 0000-0003-1519-4410

Y. Salman – 0000-0002-8564-5136

A. Mouraux – 0000-0003-1056-5980

Abstract

Background: The angular gyrus (AG) is involved in numerous cognitive processes, and structural alterations of the AG are reported in many neuropsychiatric diseases. Because abnormal excitability or connectivity of such cortical hubs could precede structural alterations and clinical symptoms, approaches assessing their functional state are needed. The combination of transcranial magnetic stimulation (TMS) with electroencephalography (EEG) can provide such functional readouts by probing how the cortex responds to direct stimulation.

Objective: To characterize TMS-evoked potentials (TEPs) elicited by AG stimulation, determine optimal stimulation parameters, and identify TEP biomarkers of AG function.

Methods: In 19 subjects, we recorded AG-TEPs using four TMS orientations and three intensities and compared their spatiotemporal features using topographic dissimilarity and microstate analyses. We also explored the link between AG-TEPs and TMS-evoked muscle activity.

Results: Early AG TEP components of interest (P25, N45) showed topographic variability dependent on stimulation parameters. The P25 topography was sensitive to TMS orientation and less to intensity, whereas the N45 topography was highly dependent on both coil orientation and intensity. However, TMS-evoked muscular activity was also dependent on coil orientation and the dominant topography of N45 was strongly related to this muscular activity, indicating that the component may reflect somatosensory-evoked responses to this peripheral activation.

Conclusions: The earliest AG TEP component P25 likely reflects neural processes triggered by direct AG activation and could provide an index of local excitability. N45 must be interpreted with caution as it may mostly reflect peripherally evoked activity. Coil orientation can be optimized to minimize muscular contractions.

Keywords

angular gyrus, transcranial magnetic stimulation, electroencephalography, TMS-evoked potentials, topographic dissimilarity, microstate analysis

Introduction

The angular gyrus (AG), one of the core nodes of the default mode network (DMN) [1-4], represents a highly connected cortical hub [5-7] implicated in a range of cognitive processes (for a review see [8]). Correspondingly, structural and connectivity abnormalities of the AG have been reported in multiple neuropsychiatric disorders including Alzheimer's disease [9-11], schizophrenia [12, 13], and amyotrophic lateral sclerosis [14, 15]. As clinical symptoms as well as structural alterations are likely to be preceded by functional changes, there is an incentive to evaluate functional properties of the AG in asymptomatic populations. This is possible by combining transcranial magnetic stimulation (TMS) with electroencephalography (EEG). While TMS selectively activates neurons of the targeted cortical region and connected areas [16, 17], EEG records the brain response to this perturbation [18, 19] and the resulting TMS-evoked potentials (TEP) can be used to characterize local excitability and connectivity [19-21].

TMS-EEG studies targeting the AG showed that it is possible to record AG TEPs that are stable across sessions and specific for individuals [22-27]. Furthermore, EEG source reconstruction revealed a target-specific propagation of activity from the stimulated AG across nodes of the DMN, thereby hinting at the utility of AG TEPs for the evaluation of this network [23]. However, to employ TEPs to study the functional state of the AG under pathological conditions, it is crucial to identify the optimal combination of stimulation parameters, characterize the evoked responses, and isolate those components that most likely reflect cortical activity triggered by direct AG activation. TMS intensity as well as the orientation and direction of the magnetic field determine which neuronal populations are stimulated and how efficiently [28, 29]. Yet, the horseshoe shape of the AG offers several possibilities to place the TMS coil, each presumably prioritizing different neuronal sub-populations. Moreover, stimulation parameters may also differentially influence undesired activation of peripheral nerves and muscles [30, 31].

Here, we aimed to describe the spatiotemporal profile of AG TEPs, to assess the impact of stimulation parameters on the response, and to identify TEP components reflecting the activity directly evoked within the AG. TMS was applied over the posterior-ventral part of the left AG, an area showing strong connectivity within the DMN [32, 33]. Four stimulation orientations and three intensities were used to record TEPs that were compared using analysis of topographic dissimilarity and microstate analysis [34, 35]. These methods allow making inferences about EEG sources based on the assumption that different topographies represent the activity of distinct cortical generators [36] and were recently successfully employed to analyze TEPs [27]. In addition, we explored the association between TMS-evoked muscular contraction and topographic features of AG TEPs.

Material and Methods

Participants

19 healthy volunteers participated in the study (9 males, mean age ± SD: 23.78 ± 3.34 years). Before enrolling, candidates filled a questionnaire to control for contraindication to experimental procedures [37]. Accepted subjects gave a written informed consent and were financially compensated for their participation. All performed procedures were conducted according to the Declaration of Helsinki and approved by the Ethical Committee of Catholic University of Louvain and University Clinics Saint-Luc.

Experimental design

TEPs were recorded from the AG using different stimulation orientations defined by the position of the TMS coil - across or along the superior temporal sulcus (STS) – and the direction of the electric current in the TMS coil - normal or reversed phases (Fig. 1c). For each of the resulting four combinations, we tested three stimulation intensities based on the individual threshold to evoke motor response at rest (resting motor threshold, rMT) – 100, 120 or 140% rMT. The experiments were conducted in two sessions (approximately 3.5 h) separated by one week, each testing one coil position (Fig. 1d).

EEG recording

The EEG was recorded with the NeurOne EEG system (Bittium NeurOne Tesla; Bittium Corporation, Oulu, Finland) using a 32 channel EEG cap mounted with TMS-compatible Ag/AgCl electrodes (EasyCap GmbH, Herrsching, Germany) (Fig. 1b). The signal was referenced to FCz and recorded at 20 kHz sampling rate with 5000 Hz low-pass filter and DC filter, with electrode impedances kept below 5kΩ. Subjects were seated in a comfortable chair and fixing their gaze to a stable point. A layer of thin plastic and another textile cap were placed over the EEG cap to minimize EEG artifacts caused by the contact of electrodes with the TMS coil and subjects were listening to a custom masking noise [38] to minimize auditory artifacts.

TMS stimulation

A 3D T1-weighted structural MRI of the head was acquired in advance (1×1×1 mm; 3 T Achieva; Philips Healthcare, Amsterdam, The Netherlands) and 3D models of the brain surface and the scalp were reconstructed in the Visor2 neuronavigation system (Visor 2.3.3; Advanced Neuro Technologies, Enschede, The Netherlands). The posterior-ventral AG was located on the brain model dorsally to the ascending branch of the STS (Fig. 1a), its position was projected on the scalp model and two TMS coil targets were created, one with the axis along the STS and the other perpendicular to it. The model was co-registered with subject's head using landmarks (nasion and tragi) and head-shape matching

[39]. The position of the head and the TMS coil was monitored with a Polaris optical tracking system (Polaris Spectra; Northern Digital Inc. Europe, Radolfzell, Germany) and the neuronavigation ensured the accurate coil placement throughout the stimulation.

Biphasic TMS pulses were delivered manually using a MagPro stimulator (MagPro X100 with MagOption; MagVenture, Farum, Denmark) with a figure-of-eight coil (75 mm; MagVenture, Farum, Denmark) placed tangentially to the scalp and aligned with the target. The intensity of stimulation was determined based on the rMT, which was identified as the minimal intensity eliciting a motor response with an amplitude ≥ 50 µV in at least 5/10 trials [29]. The average (±SD) rMT corresponded to 44.3 ± 8.5% of the maximum stimulator output (MSO). Each experimental session contained 8 blocks of 75 TMS pulses (jittered interstimulus interval 4-6 s) that were randomly assigned one of the tested stimulation intensities (Fig. 1d), delivering 100 stimuli in total for every condition.

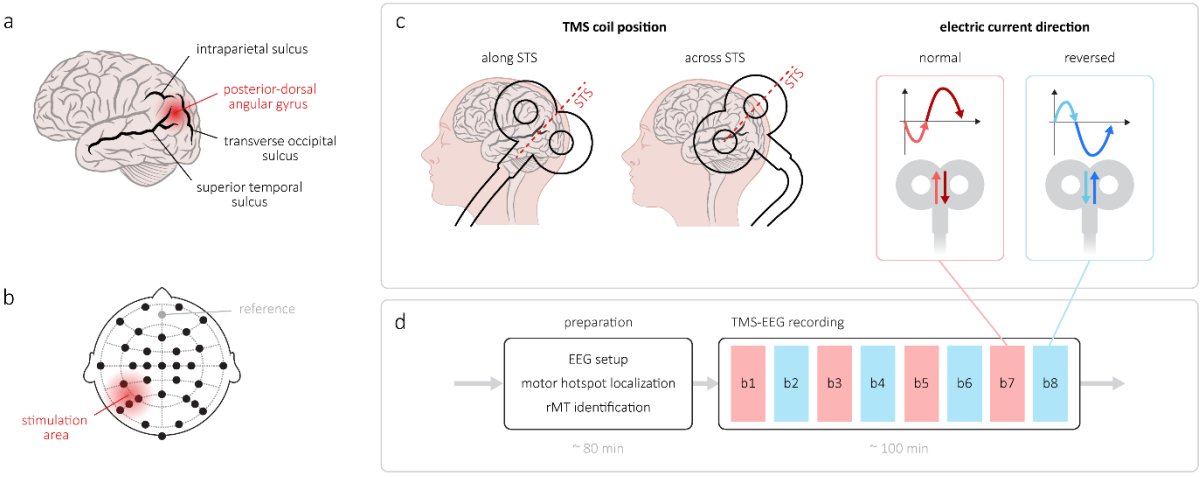

Fig. 1 Experimental design. (a) The TMS target site was located in the posterior-dorsal AG on the gyral crown defined relative to the position of the most prominent sulci marked in the figure. (b) EEG layout used in the study comprised 32 active electrodes (black), the reference is shown in grey, the red shading approximates the area under the TMS coil. (c) Four tested stimulation orientations were defined as the combination of two different TMS coil positions – along and across the axis of the superior temporal sulcus (STS) and two directions of the electric current in the coil – normal (prominent second phase in dark red) and reversed (prominent phase in dark blue). (d) One experimental session contained 8 blocks of TMS-EEG (each approximately 6.5 mins long) with the coil position constant but the current in the coil alternating between the blocks.

Data pre-processing

EEG recordings were pre-processed offline using Matlab (MathWorks, Inc., Natick, Massachusetts, United States), Letswave 6 (an open-source EEG/EMG signal processing toolbox, https://www.letswave.org/) and custom scripts following the pipeline introduced by Rogasch [40].

The signal was re-referenced to the common average, epoched (-1000 to 2000 ms relative TMS), and the DC shift and linear trend were removed. The large muscle artifact was replaced by cubic interpolation (-5 to +10 ms) and the signal was downsampled to 2 kHz. A first round of Independent

Component Analysis (ICA, FastICA algorithm [41]) was performed to remove components containing the sharp leftover tail of the muscle artifact. Data were bandpass filtered (0.1-80 Hz, Butterworth, 4th order) and notch filtered (50 Hz, FFT linear filter, width 2 Hz, slope 2 Hz). All epochs were visually inspected to discard those containing excessive noise, the average final number of epochs per condition was 83.7 ± 7.9.

A second round of ICA was used to remove remaining artifacts, such as eye movements, tonic muscle activity and electrode noise, as well as the remains of the muscular artifact. Suspicious components were identified with the Multiple Artifact Rejection Algorithm (MARA) [42] and evaluated visually based on their topography, time course and frequency content. For detailed information on this step, please consult the supplementary material of [43].

Finally, the TEPs were baseline corrected (-200 to -5 ms) and group averaged.

Data analysis and statistics

AG TEPs were evaluated between 10 and 300 ms post stimulus. The peaks within this window were identified in the group average waveforms separately for each stimulation orientation (intensities pooled) and labelled according to their prominent polarity (P = positive, N= negative) and approximate peak latency (ms). Latencies were extracted from local maxima of the Global Field Power (GFP; Equation 1) [44].

Topographic analysis was performed in Ragu (Matlab toolbox for randomization-based analysis of EEG event-related potentials [45]) and using custom Matlab scripts. First, outliers were identified based on the Mahalanobis distance between subjects [46] and excluded. The subsequent steps followed the pipeline indicated in [47], always using 5000 permutations for the randomization and the level of significance set to 0.05. Here, we provide a brief outline of the process and invite the reader to see [27] for a detailed description. Because topographic analysis operates with normalized data, it disregards potential differences in TEP amplitude. Therefore, we additionally evaluated the influence of stimulation parameters on the magnitude of AG TEP components. These results are reported in the Supplementary materials.

Planned comparisons. The effect of two factors on AG TEPs as well as their interaction were evaluated: (1) *TMS orientation*, with four levels corresponding to different combinations of TMS coil position and electric current direction (*along-normal*, *along-reversed*, *across-normal*, and *across-reversed*); (2) *TMS intensity,* with three levels (100, 120, and 140% rMT). All comparisons were made while considering the spatiotemporal features of TEPs (analysis of topographic dissimilarity and microstate analysis) as well their magnitude (analysis of GFP amplitude).

Test for topographic consistency (TCT). TCT was conducted separately for each tested condition to identify time intervals showing significant topographic homogeneity across individuals. The GFP of

the group average TEP was used as a quantifier and tested against an empirically obtained distribution computed from signals spatially scrambled at subject level.

Analysis of topographic similarity. TEP topographies were compared using the measure of Global Dissimilarity (DISS; Equation 2) introduced by [44]. For each planned comparison, DISS was calculated based on group average TEPs (normalized at subject level by GFP) and a point-by-point statistical randomization test (TANOVA) was conducted to determine the time intervals of significant difference. The clusters of significant p values were corrected for multiple comparisons by applying a Ragu procedure called "Global Duration Statistics", which determines the minimum necessary number of consecutive significant time points based on the data obtained by randomization. For each factor, we calculated the momentary percentage of total explained variance (%EV), which allowed us to identify temporal maxima of topographic dissimilarity. Mean TEP topographies were extracted at these latencies and post-hoc comparisons were performed using channel-wise paired t-tests. Obtained t values were plotted as t-maps to describe the distribution and magnitude of topographic differences. The significance level was Bonferroni corrected, only significant comparisons were reported.

Microstate analysis. Microstate analysis was used to evaluate temporal properties of observed topographic differences. First, the optimal number *n* of microstate classes was determined using the cross-validation method [34]. In the next step, *n* microstate classes were identified using the k-means clustering algorithm [48] with 250 restarts. Each timepoint within each group average TEP was then labelled with the class map that yielded the highest spatial correlation with the momentary topography, thereby segmenting the waveform into intervals of dominance of one of the *n* microstate classes. We then compared temporal properties (*onset*, *offset*, and *mean duration*) of each class across datasets. For each comparison and microstate, we quantified the observed effect by computing its variance across levels and tested it against an empirically obtained distribution of values true under the null hypothesis.

$$GFP(t) = \sqrt{\frac{\sum_{j=1}^{n}(u_j(t) - \bar{u}(t))^2}{n}} \quad (1) \qquad DISS_{u,v}(t) = \sqrt{\frac{1}{n} \cdot \sum_{i=1}^{n}\left(\frac{u_i(t)}{GFP_u(t)} - \frac{v_i(t)}{GFP_v(t)}\right)^2} \quad (2)$$

Equations of (1) Global Field Power GFP and (2) Global Dissimilarity DISS. Calculated at each timepoint t, n is the number of electrodes, u_i and v_i represent the voltage measured at one electrode in two different conditions, while $\bar{u}$ is the mean voltage in a single condition.

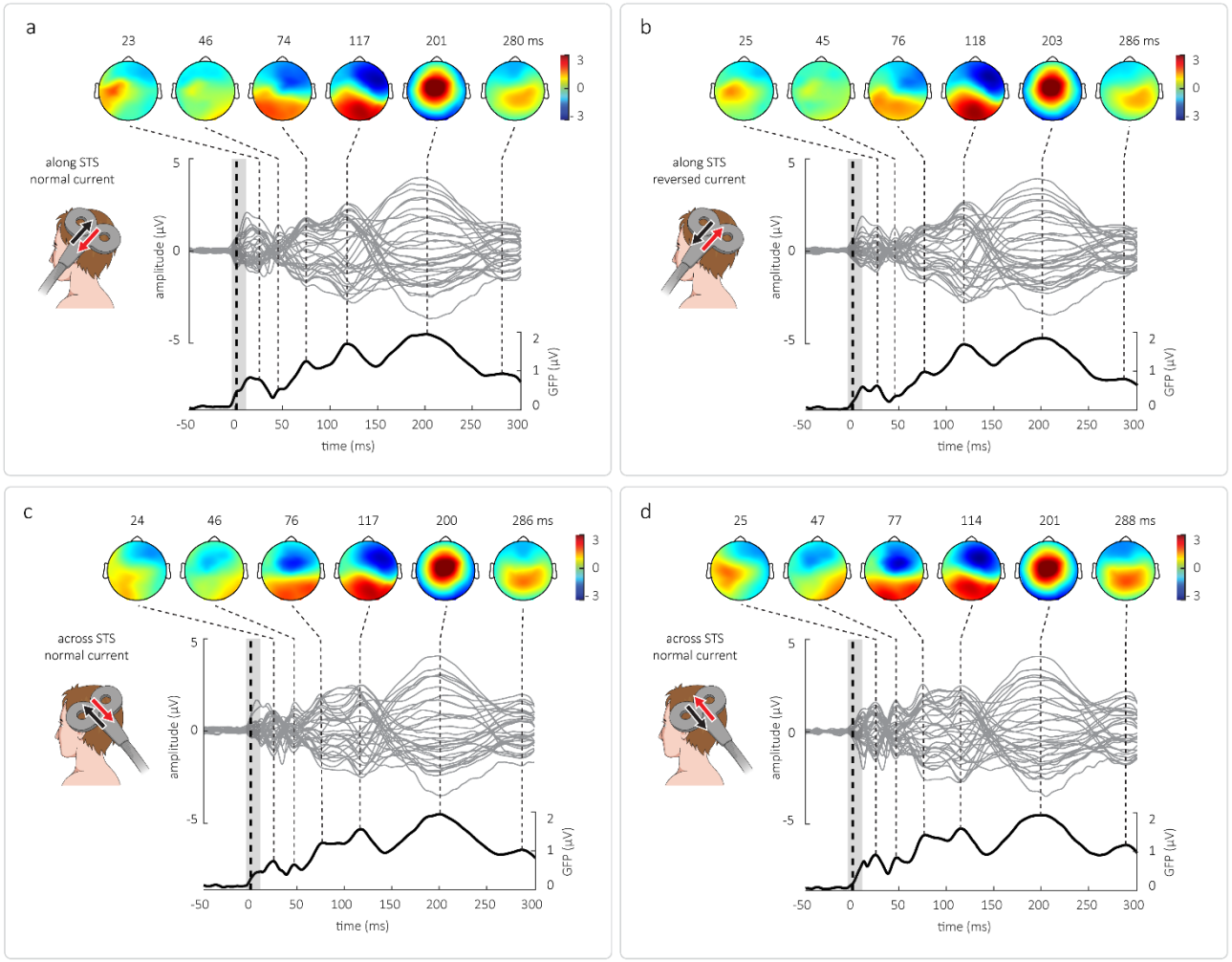

Fig. 2 Spatiotemporal profile of AG TEPs obtained with the TMS coil placed along (a, b) or across (c, d) STS and the current flowing in the normal (a, c) or reversed (b, d) direction. For the purposes of visualization, TEPs evoked by all three intensities were averaged. The current direction in the coil is marked by a black (phase 1) and a red (phase 2) arrow. Grey lines in the middle section represent the signal of all recorded EEG channels, the TMS stimulus is denoted by a thick dashed line and the interpolated interval is shaded in light grey. The GFP of the average signal is plotted at the bottom and identified TEP components are marked by dotted lines that are associated with peak topographies displayed in the upper section; peak latencies in ms post stimulus are noted above.

Results

In the text, we will refer to TEP datasets by the combination of stimulation parameters used: *orientation (along/across) – current (normal/reversed) – intensity (100/120/140)*.

Spatiotemporal characteristics of AG TEPs

One individual was identified as outlier and excluded (final n = 18) and remaining datasets were tested for topographic consistency, which was confirmed for the whole duration of the analyzed time window (10 – 300 ms post stimulus) with the exception of five short intervals: 34 – 51 ms in *along-reversed-120*, 12 – 19 and 32.5 – 39 ms in *along-reversed-140*, 50.5 – 61 ms in *across-normal-100* and

10 – 14.5 ms in *across-normal-140*. These epochs were not removed from subsequent analysis but were considered when interpreting the results.

AG TEPs of all conditions comprised six components that were distinguishable already at the individual subject level. To describe their general properties, data from the three stimulation intensities were pooled together for each stimulation orientation (Fig. 2). Peak latencies of these components as identified in the group average GFP were similar across all four datasets, whereas their associated topographies visibly differed in the three earlier peaks (Fig. 2, upper rows). For future reference, AG TEP components were labelled consistently in all conditions: P25, N45, N75, N100, P200 and P280.

comparison		%EV peak latency (ms)	t maximum		t minimum		significance
			value	channel	value	channel	
TMS orientation							
current direction	*along-normal*	43	7.55	O2	-9.92	F3	n.s.
	– along-reversed	81	5.00	C2	-6.98	Fz	n.s.
	across-normal	43	7.20	F3	-5.26	P8	n.s.
	– across-reversed	81	10.62	FP2	-11.39	C3	n.s.
coil orientation	*along-normal*	43	23.22	C1	-9.56	F7	p < 0.01
	– across-normal	81	19.35	C3	-16.31	T8	p < 0.01
	along-normal	43	21.14	C3	-16.17	P8	p < 0.001
	– across-reversed	81	11.07	FC1	-13.81	CP6	n.s.
	along-reversed	43	22.55	C1	-11.07	CP6	p < 0.01
	– across-normal	81	22.24	C3	-15.02	T8	p < 0.001
	along-reversed	43	24.72	FC1	-18.74	P4	p < 0.001
	– across-reversed	81	15.69	FC1	-11.50	FC6	n.s.
TMS intensity							
120 – 100% rMT		47	11.3	O1	-22.56	FC1	p < 0.001
		258	16.48	CP2	-15.14	P7	n.s.
140 – 120% rMT		47	11.93	CP6	-16.13	FC1	p < 0.01
		258	18.49	Pz	-26.01	F8	p < 0.001
Interaction: comparison at 140% rMT							
current direction	*along-normal – along-reversed*	80	5.64	F8	-4.60	Fz	n.s.
	across-normal – across-reversed		6.96	FP2	-7.93	F4	n.s.
coil orientation	*along-normal – across-normal*		22.35	C1	-21.65	FC6	p < 0.001
	along-normal – across-reversed		19.50	CP1	-25.17	FC6	p < 0.001
	along-reversed – across-normal		22.39	C1	-19.30	CP6	p < 0.001
	along-reversed – across-reversed		-17.37	C3	-20.38	FC6	p < 0.01

Table 1 Post-hoc evaluation of topographic dissimilarity. The significance marks the p value obtained by a paired t-test comparing two given datasets.

Topographic dissimilarity

Effect of stimulation orientation. TANOVA identified two intervals of significant dissimilarity: 10-59 ms and 66-106 ms. Within these intervals, local maxima of total explained variance (%EV) were found at 22, 43 and 81 ms post stimulus (Fig. 3a). These latencies, corresponding to AG TEP components P25, N45 and N75, were then used to extract mean topographies for all compared datasets (Fig. 3b). Six post-hoc paired t-tests were performed at all three latencies but only comparisons at 43 and 81 ms were found significant. In both cases, a significant difference was observed between conditions of opposite coil position (*along* – *across,* t-maps shown in Fig. 3c), while no significance was found for the effect of current direction. At 43 ms (N45), the t-maps of all *along* – *across* t-tests showed very similar patterns, with a positivity centro-anterior on the stimulated hemisphere. The t-value distribution was less uniform at 81 ms (N75) but still featured in all four cases a centro-frontal ipsilateral positivity. The locations of t-map maxima and minima and the associated t-values are summarized in Table 1.

Effect of stimulation intensity. TANOVA identified three intervals during which the topography significantly changed with the increasing stimulation intensity: 38-70 ms, 74.5-118 ms and 224-300 ms. Local maxima of %EV were found at 47, 92 and 258 ms, corresponding to AG TEPs components N45, N75 and P280 (Fig. 3d,e). At each %EV peak latency, post-hoc t-tests were performed to compare datasets evoked by two neighbouring stimulation intensities. At 47 ms (N45), the topography changed significantly between 100 and 120% rMT as well as between 120 and 140% rMT and both associated t-maps had a similar distribution pattern with the minimum localized frontally at the stimulated hemisphere and the maximum posteriorly at the opposite hemisphere. In addition, the topography was found significantly different when comparing datasets evoked by 120 and 140% rMT at 258 ms (P280), with the corresponding t-map showing an increase in positive values posterio-centrally (Fig. 3f, Table 1).

Interaction of stimulation orientation and intensity. One interval at 71.5-96 ms was retained by TANOVA as significant, with a local %EV maximum at 80 ms corresponding to the component N75 (Fig. 3g, h). Six post-hoc t-tests were used to compare all datasets at 100% rMT and at 140% rMT. While neither of the comparisons at 100% rMT proved significant, highly significant differences were found at 140% rMT when topographies with opposite coil position (*along* - *across*) were compared. All t-maps showed similar patterns, with positivity at the stimulated hemisphere (Fig. 3i, Table 1).

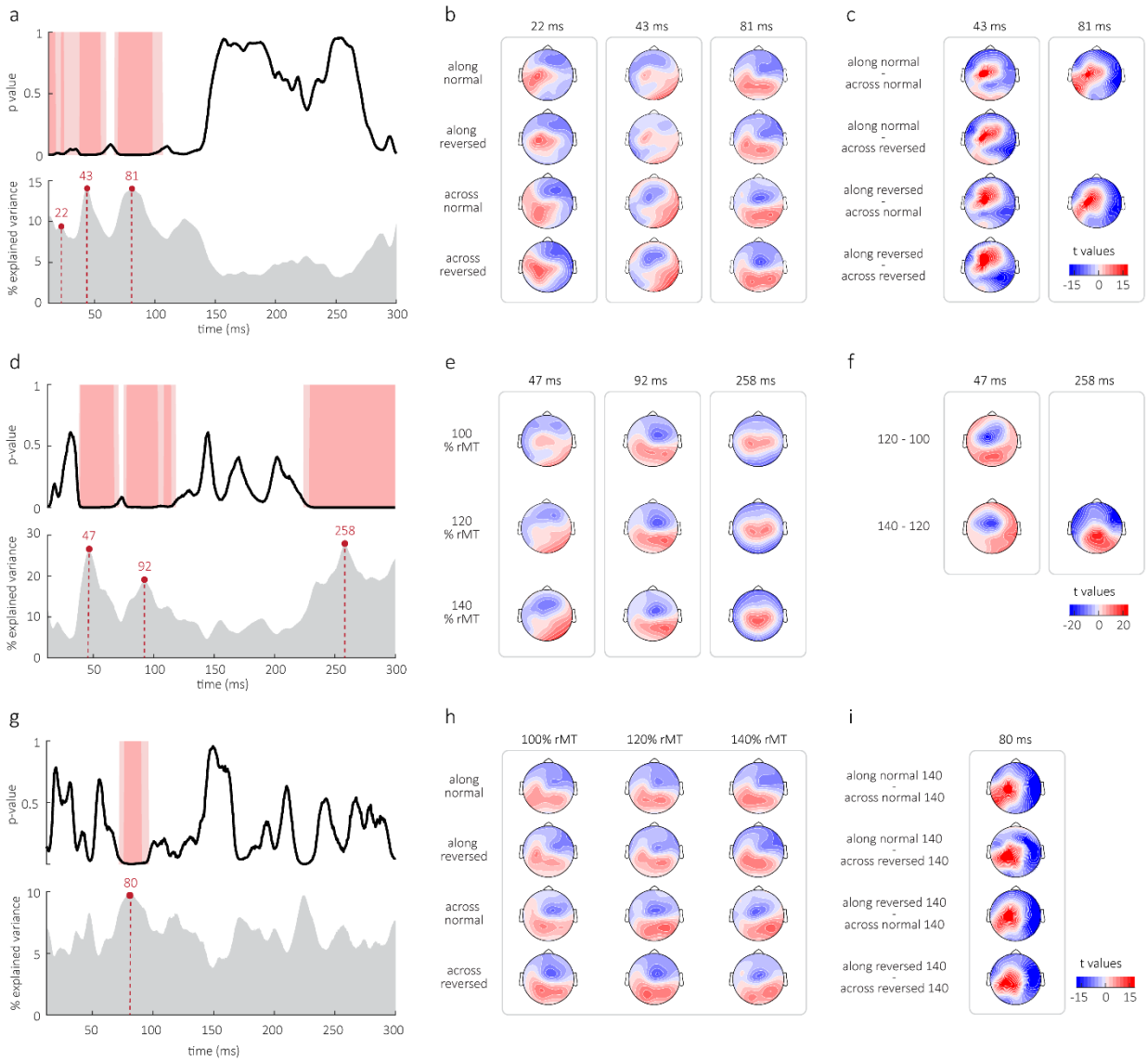

Fig. 3 Analysis of topographic dissimilarity for different stimulation orientation (a, b, c), intensity (d, e, f) and the interaction of both factors (g, h, i). (a, d, g) Upper plots show p-values obtained by TANOVA in the analyzed time window (10 – 300 ms). Areas shaded in light pink correspond to intervals of $p < 0.05$, dark pink areas to intervals of $p < 0.01$. Bottom plots show percentage of explained variance attributed to given factor at each timepoint, peak latencies are marked by red dotted lines. (b, e, h) Mean topographies normalized to GFP that are associated to peak %EV latencies. (c, f, i) T-maps show the distribution of t-values obtained in post-hoc comparisons. Only the significant comparisons are shown.

Microstate analysis

The model (92.3% explained total variance) yielded six microstate classes (Fig. 4a) and attributed a prominent topography to each TEP component (Fig. 4b). Intervals of low TEP amplitude, particularly around 50 ms, were associated with rapidly switching short-lasting microstates, suggesting moments of topographic instability or transition (Fig. 4b,c). Analysis of temporal features was performed for all microstate classes, significant results were obtained for classes 2, 3 and 4.

Microstate class 2 appeared at the falling slope of component N100 and in most *along* datasets and in *across-100* datasets, it also appeared at the rising slope of N75. This was reflected in statistically

significant effect of both orientation ($p < 0.001$) and intensity ($p < 0.001$) on its overall duration. We observed that class 2 lasted longer in *along-normal* and *along-reversed* datasets (on average 23 and 45 ms) than in *across-normal* and *across-reversed* datasets (15 and 16 ms). Its duration was reduced with increasing stimulation intensity (100% rMT – 40 ms; 120% rMT – 18.5 ms; 140% rMT – 17.5 ms) and this trend was more pronounced in *across* datasets (borderline significant).

Microstate class 3 represented the peak topography of both N75 and N100 in all datasets except for *across-normal-140* and *across-reversed-140*, where it was replaced at N75 latency by microstate class 4. While the occurrence of class 3 in *along* datasets changed only slightly with stimulation intensity, we saw its progressive suppression in *across* datasets as the intensity increased. This corresponds to the significant effect of orientation-intensity interaction on class 3 onset. Mean onset (ms) for 100 / 120 / 140% rMT: *along-normal* – 59.5 / 60 / 51; *along-reversed* – 66 / 65 / 49; *across-normal* – 62 / 55 / 114; *across-reversed* – 49 / 53 / 109.

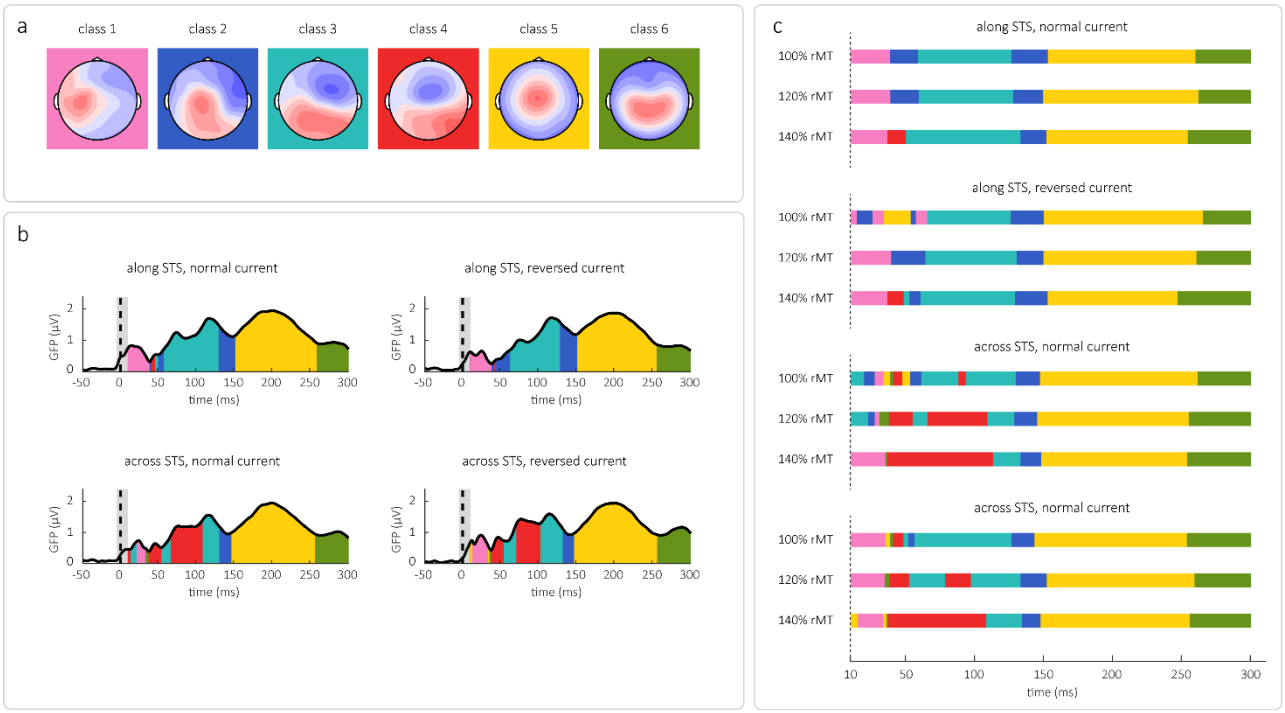

Fig. 4 Microstate analysis. (a) 6 microstate class maps generated by the model with assigned colors. (b) GFP plots of TEPs averaged across tested intensities for each stimulation orientation are split into intervals corresponding to microstate classes to illustrate how microstates correspond to TEP components. (c) Microstate sequences of TEPs of all conditions; timepoints labelled with different microstate classes are color-coded according to panel a.

The most pronounced differences between tested conditions were observed in temporal characteristics of microstate class 4. While it was missing in most *along* datasets, only appearing in a short interval in *along-normal-140* and *along-reversed-140* at latencies corresponding to N45, it was detectable in all *across* datasets where it also gained with the increasing stimulation intensity over the class 3 at the latency of N75. This is reflected in the significant effect of stimulation orientation and intensity, as well as their interaction, on the overall duration of class 4. Mean duration (ms) for 100 / 120 / 140% rMT: *along-normal* – 0 / 0 / 13; *along-reversed* – 0 / 0 / 12; *across-normal* – 12 / 61 / 77; *across-reversed* – 8 / 33 / 71. In addition, we found a significant effect of stimulation orientation on the class 4 offset. Mean offset (ms): *along-normal* – 46; *along-reversed* – 44; *across-normal* – 109; *across-reversed* – 103.

Contribution of muscular contraction

During the study, a suspicion was raised that topographic differences observed between *along* and *across* AG TEPs may be related to the characteristics of face muscle contractions directly evoked by TMS rather than differential activation of target brain networks. Therefore, an exploratory analysis was carried out to evaluate the contribution of this muscular artifact. A high-amplitude evoked potential peaking within 10 ms post stimulus and showing typical peripheral distribution (Fig. 5a) was recovered from untreated EEG data (TMS artifact was removed between -2 and 3 ms) and attributed to the muscular contraction. Its magnitude was quantified at the subject level as the average GFP_{muscle} at 3-10 ms post stimulus (only electrodes from the stimulated hemisphere were included; Fig. 5b). At this point, two additional subjects were identified as outliers based on their GFP_{muscle} values and removed (final n_{muscle} = 16). Group visualization revealed that *across* datasets were associated with a larger muscular artifact that showed a steeper increase with stimulation intensity as compared to *along* datasets, while the influence of current direction apparently less important (Fig. 5c). Mean GFP_{muscle} values are summarized in Table 2.

Microstate analysis indicated that the most remarkable difference between *along* and *across* datasets was the occurrence of the topographic pattern attributed to the microstate class 4 at the N45 latency. To investigate the association of the muscular artifact magnitude and this specific topography, all data were grouped by coil position, sorted, and split into four categories of increasing GFP_{muscle} (Fig. 5d, upper panels). TEP topographies was extracted at 45 ms from processed datasets averaged within each category. We observed that in both *along* and *across* datasets, larger muscular artifacts were associated with more prominent class 4 topography (Fig. 5d, lower panels). Its appearance was less pronounced in *along* datasets, which corresponded to a comparatively weaker average muscular artifact.

dataset		average GFP_{muscle}	dataset		average GFP_{muscle}
orientation	**intensity** (%rMT)	(µV ± SEM)	**orientation**	**intensity** (%rMT)	(µV ± SEM)
along normal	100	21.46 ± 7.62	across normal	100	42.27 ± 14.48
	120	37.55 ± 12.52		120	62.01 ± 15.37
	140	59.18 ± 18.52		140	100.45 ± 19.30
along reversed	100	22.28 ± 8.70	across reversed	100	47.29 ± 15.43
	120	25.62 ± 6.98		120	72.44 ± 19.78
	140	38.76 ± 11.25		140	117.24 ± 28.23

Table 2 Magnitude of TMS-evoked muscular contraction.

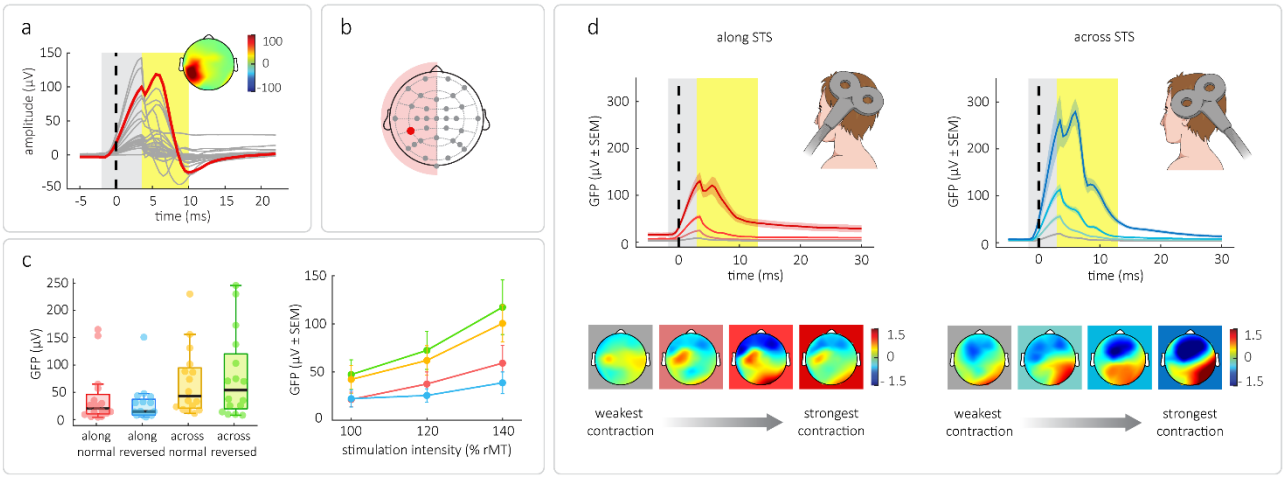

Fig. 5 Quantification of evoked muscular contraction. (a) Average signal from all datasets showing the time-course and topography of the artifact attributed to muscular contraction; grey lines represent the signal of all electrodes, CP5 is highlighted in red. The time interval of TMS artifact interpolation is shaded in light grey, yellow area represents the time of interest over which the GFP_{muscle} was calculated. The topography was extracted at the latency of the CP5 peak (5 ms post stimulus). (b) EEG layout used in the study with the CP5 electrode highlighted in red marking the approximate site of stimulation. Only the signal from channels at the left (stimulated) hemisphere were used to calculate mean GFP_{muscle} used to quantify the strength of muscular twitch. (c) Mean group values of GFP_{muscle}; red – *along-normal*, blue – *along-reversed*, yellow – *across-normal*, green – *across-reversed*. Left panel shows individual data with all intensities averaged; black bars mark median values, box whiskers connect lower and upper quartiles to nonoutlier maxima and minima. Right panel shows group average values (± SEM) for all datasets. (d) Increasing muscular artifact in *along* (red, upper panel) and *across* (blue, upper panel) datasets with the corresponding topography at 45 ms (lower panels). The interval of TMS artifact interpolation is shaded in light grey, yellow area represents the time of interest over which the GFP_{muscle} was calculated.

Discussion

In the present work, we characterized the spatiotemporal profile of AG TEPs and showed that its topographic features depend on TMS coil orientation and stimulation intensity. Specifically, when investigating the effect of coil orientation, we found topographic dissimilarity across tested conditions at latencies corresponding to components P25, N45 and N75, indicating that different cortical sources were active or that the same sources contributed differently to the global activity. However, it appears that this variability cannot be solely attributed to differences in activity of the stimulated area.

One major concern when interpreting TEPs is the inevitable contamination by peripherally evoked sensory potentials (PEPs) [30, 49]. The magnetic field and coil vibration activate a range of receptors in the soft tissues of the head, thereby triggering somatosensory-evoked brain potentials (SEPs), while the clicking sound of TMS produces auditory-evoked potentials (AEPs). By comparing active TMS with sham stimulation, multiple studies showed that PEP contribution to TEPs increases with time and must be considered as soon as 50-60 ms post stimulus [26, 49-53]. Therefore, P25 and N45 should be the most relevant components of AG TEPs to probe the functional status of the AG.

Several arguments indicate that P25 is likely to reflect activity due to direct cortical activation of the AG network. We previously compared TEPs evoked from the primary motor cortex and the AG (coil placed across STS) and found that the P25 topography is highly target specific [27]. Here, we observed significant topographic dissimilarity of P25 of AG TEPs evoked by different stimulation orientation, yet the patterns were similar enough to be pooled into a single microstate. This subtle variability could be explained by differential engagement of local neuronal sub-populations depending on their sensitivity to different features of the induced electric field. Moreover, another recent study succeeded to locate P25 cortical generators in the stimulated AG as well as the ipsilateral ventral medial prefrontal cortex (vmPFC) [23], an area also belonging to the DMN [54]. Therefore, P25 of AG TEPs likely represents a valuable non-invasive biomarker of the functional state of the AG network.

By contrast, our data suggest that the later component N45 might be prone to contamination by somatosensory-evoked input triggered the TMS-evoked twitch of head muscles. When the TMS coil is placed over a head muscle, the stimulation triggers a muscular contraction [55] which, in turn, activates mechano-sensitive somatosensory afferents. Because coil placement determines the character of muscle activation, distinct coil orientations are likely associated with differences in the strength of muscular activation and somatosensory feedback, leading to variable degrees of TEP contamination by somatosensory-evoked cortical activity. Such difference might be especially pronounced when stimulating targets with lateral projection on the scalp, such as the AG. Indeed, we observed that the muscular contraction was stronger when TMS stimulation was delivered *across* as compared to *along* the STS and augmented with increasing stimulation intensity. Most importantly,

the effects of TMS coil orientation and stimulation intensity on the N45 topography followed the effects on TMS-evoked muscular activity.

Furthermore, the microstate analysis revealed that N45 elicited by AG stimulation *across* the STS was dominated by a bipolar topographic pattern (microstate class 4) centred over the contralateral hemisphere, whose occurrence and duration increased with stimulation intensity. This topography bears a striking resemblance to that of mid-latency SEPs evoked by electrical stimulation of mixed peripheral nerves of the face accompanied by a muscle twitch [56-58]. Independently of coil position, this pattern became more pronounced as the magnitude of the muscular artifact increased. Moreover, considering the influence of individual anatomy on muscular contractions, variable occurrence of muscular activation could explain the inter-subject topographic inconsistency of the N45 component, previously also described for motor cortex TEPs [27]. Therefore, TEP changes at the latency of N45 should be interpreted with caution, especially when simultaneous changes in evoked muscular activity occur.

Conclusion

In summary, we show that topographic features of early AG TEPs are dependent on TMS stimulation parameters, thus reflecting differential engagement of underlying brain sources. We conclude that the earliest component P25 of AG TEPs likely corresponds to brain activity evoked by direct activation of the AG and as such could serve as a biomarker of excitability within the AG and the connected DMN. In contrast, the subsequent component N45 seems to be influenced by the presence of TMS-evoked peripheral muscle activity and should be interpreted with caution. While all tested TMS coil positions efficiently activate the AG, placing the coil along STS minimizes muscular contractions and should be preferred when recording AG TEPs.

Funding

Presented work was supported by the Fonds de la Recherche Scientifique (FNRS) of which D. Sulcova is a research fellow.

Data and code availability

All data and code can be made available upon a reasonable request to the corresponding author.

CRediT authorship contribution statement

Dominika Sulcova: Conceptualization, Methodology, Investigation, Software, Formal analysis, Writing - original draft, Writing – review & editing, Visualization; *Yasmine Salman:* Methodology, Investigation; *Adrian Ivanoiu:* Resources, Funding acquisition, Supervision; *André Mouraux*: Resources, Funding acquisition, Supervision, Writing – review & editing

References

1. Buckner, R.L. and L.M. DiNicola, *The brain's default network: updated anatomy, physiology and evolving insights.* Nature Reviews Neuroscience, 2019. **20**(10): p. 593-608.
2. Buckner, R.L., J.R. Andrews-Hanna, and D.L. Schacter, *The brain's default network: anatomy, function, and relevance to disease.* Annals of the new York Academy of Sciences, 2008. **1124**(1): p. 1-38.
3. Greicius, M.D., et al., *Functional connectivity in the resting brain: a network analysis of the default mode hypothesis.* Proceedings of the National Academy of Sciences, 2003. **100**(1): p. 253-258.
4. Shehzad, Z., et al., *The resting brain: unconstrained yet reliable.* Cerebral cortex, 2009. **19**(10): p. 2209-2229.
5. Hagmann, P., et al., *Mapping the structural core of human cerebral cortex.* PLoS biology, 2008. **6**(7): p. e159.
6. Tomasi, D. and N.D. Volkow, *Association between functional connectivity hubs and brain networks.* Cerebral cortex, 2011. **21**(9): p. 2003-2013.
7. Kernbach, J.M., et al., *Subspecialization within default mode nodes characterized in 10,000 UK Biobank participants.* Proceedings of the National Academy of Sciences, 2018. **115**(48): p. 12295-12300.
8. Seghier, M.L., *The angular gyrus: multiple functions and multiple subdivisions.* The Neuroscientist, 2013. **19**(1): p. 43-61.
9. Jagust, W., et al., *Brain imaging evidence of preclinical Alzheimer's disease in normal aging.* Annals of Neurology: Official Journal of the American Neurological Association and the Child Neurology Society, 2006. **59**(4): p. 673-681.
10. Smith, C., et al., *Brain structural alterations before mild cognitive impairment.* Neurology, 2007. **68**(16): p. 1268-1273.
11. Berron, D., et al., *Medial temporal lobe connectivity and its associations with cognition in early Alzheimer's disease.* Brain, 2020. **143**(4): p. 1233-1248.
12. Chahine, G., et al., *Disruptions in the left frontoparietal network underlie resting state endophenotypic markers in schizophrenia.* Human Brain Mapping, 2017. **38**(4): p. 1741-1750.
13. Torrey, E.F., *Schizophrenia and the inferior parietal lobule.* Schizophrenia research, 2007. **97**(1-3): p. 215-225.
14. Sakurai, T., et al., *Dysfunction of the left angular gyrus may be associated with writing errors in ALS.* Amyotrophic lateral sclerosis and frontotemporal degeneration, 2021. **22**(3-4): p. 267-275.
15. Agosta, F., et al., *Divergent brain network connectivity in amyotrophic lateral sclerosis.* Neurobiology of aging, 2013. **34**(2): p. 419-427.
16. Hallett, M., *Transcranial magnetic stimulation: a primer.* Neuron, 2007. **55**(2): p. 187-199.
17. Barker, A.T., R. Jalinous, and I.L. Freeston, *Non-invasive magnetic stimulation of human motor cortex.* The Lancet, 1985. **325**(8437): p. 1106-1107.

18. Ilmoniemi, R.J. and D. Kičić, *Methodology for combined TMS and EEG.* Brain topography, 2010. **22**(4): p. 233.
19. Bergmann, T.O., et al., *Combining non-invasive transcranial brain stimulation with neuroimaging and electrophysiology: current approaches and future perspectives.* NeuroImage, 2016. **140**: p. 4-19.
20. Ferreri, F. and P.M. Rossini, *TMS and TMS-EEG techniques in the study of the excitability, connectivity, and plasticity of the human motor cortex.* Reviews in the Neurosciences, 2013. **24**(4): p. 431-442.
21. Mäki, H. and R.J. Ilmoniemi, *The relationship between peripheral and early cortical activation induced by transcranial magnetic stimulation.* Neuroscience letters, 2010. **478**(1): p. 24-28.
22. Ross, J.M., et al., *A structured ICA-based process for removing auditory evoked potentials.* Scientific Reports, 2022. **12**(1): p. 1-19.
23. Ozdemir, R.A., et al., *Individualized perturbation of the human connectome reveals reproducible biomarkers of network dynamics relevant to cognition.* Proceedings of the National Academy of Sciences, 2020. **117**(14): p. 8115-8125.
24. Ozdemir, R.A., et al., *Cortical responses to noninvasive perturbations enable individual brain fingerprinting.* Brain stimulation, 2021. **14**(2): p. 391-403.
25. Lauro, L.J.R., et al., *TDCS increases cortical excitability: Direct evidence from TMS–EEG.* Cortex, 2014. **58**: p. 99-111.
26. Freedberg, M., et al., *Identifying site-and stimulation-specific TMS-evoked EEG potentials using a quantitative cosine similarity metric.* Plos one, 2020. **15**(1): p. e0216185.
27. Sulcova, D., et al., *Investigating the origin of TMS-evoked brain potentials using topographic analysis.* Brain Topography, 2022: p. 1-16.
28. Siebner, H.R., et al., *Transcranial magnetic stimulation of the brain: What is stimulated?–a consensus and critical position paper.* Clinical Neurophysiology, 2022.
29. Rossini, P.M., et al., *Non-invasive electrical and magnetic stimulation of the brain, spinal cord, roots and peripheral nerves: basic principles and procedures for routine clinical and research application. An updated report from an IFCN Committee.* Clinical Neurophysiology, 2015. **126**(6): p. 1071-1107.
30. Conde, V., et al., *The non-transcranial TMS-evoked potential is an inherent source of ambiguity in TMS-EEG studies.* Neuroimage, 2019. **185**: p. 300-312.
31. Mutanen, T., H. Mäki, and R.J. Ilmoniemi, *The effect of stimulus parameters on TMS–EEG muscle artifacts.* Brain stimulation, 2013. **6**(3): p. 371-376.
32. Uddin, L.Q., et al., *Dissociable connectivity within human angular gyrus and intraparietal sulcus: evidence from functional and structural connectivity.* Cerebral cortex, 2010. **20**(11): p. 2636-2646.
33. Mars, R.B., et al., *Diffusion-weighted imaging tractography-based parcellation of the human parietal cortex and comparison with human and macaque resting-state functional connectivity.* Journal of Neuroscience, 2011. **31**(11): p. 4087-4100.
34. Koenig, T., et al., *A tutorial on data-driven methods for statistically assessing ERP topographies.* Brain topography, 2014. **27**(1): p. 72-83.
35. Šulcová, D., et al., *Investigating the origin of TMS-evoked brain potentials using topographic analysis.* 2022.
36. Michel, C.M., et al., *EEG source imaging.* Clinical neurophysiology, 2004. **115**(10): p. 2195-2222.
37. Rossi, S., et al., *Safety, ethical considerations, and application guidelines for the use of transcranial magnetic stimulation in clinical practice and research.* Clinical neurophysiology, 2009. **120**(12): p. 2008-2039.
38. Russo, S., et al., *TAAC-TMS Adaptable Auditory Control: a universal tool to mask TMS clicks.* Journal of Neuroscience Methods, 2022. **370**: p. 109491.

39. Gugino, L.D., et al., *Transcranial magnetic stimulation coregistered with MRI: a comparison of a guided versus blind stimulation technique and its effect on evoked compound muscle action potentials.* Clinical neurophysiology, 2001. **112**(10): p. 1781-1792.
40. Rogasch, N.C., et al., *Removing artefacts from TMS-EEG recordings using independent component analysis: importance for assessing prefrontal and motor cortex network properties.* Neuroimage, 2014. **101**: p. 425-439.
41. Hyvärinen, A. and E. Oja, *Independent component analysis: algorithms and applications.* Neural networks, 2000. **13**(4-5): p. 411-430.
42. Winkler, I., S. Haufe, and M. Tangermann, *Automatic classification of artifactual ICA-components for artifact removal in EEG signals.* Behavioral and Brain Functions, 2011. **7**(1): p. 1-15.
43. Sulcova, D., et al., *Evaluation of GABAAR-mediated inhibition in the human brain using TMS-evoked potentials.* bioRxiv, 2022: p. 2022.10.31.514225.
44. Lehmann, D. and W. Skrandies, *Reference-free identification of components of checkerboard-evoked multichannel potential fields.* Electroencephalography and clinical neurophysiology, 1980. **48**(6): p. 609-621.
45. Koenig, T., et al., *Ragu: a free tool for the analysis of EEG and MEG event-related scalp field data using global randomization statistics.* Computational intelligence and neuroscience, 2011. **2011**.
46. Wilks, S.S., *Multivariate statistical outliers.* Sankhyā: The Indian Journal of Statistics, Series A, 1963: p. 407-426.
47. Habermann, M., et al., *A student's guide to randomization statistics for multichannel event-related potentials using ragu.* Frontiers in neuroscience, 2018. **12**: p. 355.
48. Murray, M.M., D. Brunet, and C.M. Michel, *Topographic ERP analyses: a step-by-step tutorial review.* Brain topography, 2008. **20**(4): p. 249-264.
49. Biabani, M., et al., *Characterizing and minimizing the contribution of sensory inputs to TMS-evoked potentials.* Brain stimulation, 2019. **12**(6): p. 1537-1552.
50. Gordon, P.C., et al., *Recording brain responses to TMS of primary motor cortex by EEG–utility of an optimized sham procedure.* NeuroImage, 2021. **245**: p. 118708.
51. Gordon, P.C., et al., *Comparison of cortical EEG responses to realistic sham versus real TMS of human motor cortex.* Brain stimulation, 2018. **11**(6): p. 1322-1330.
52. Chowdhury, N.S., et al., *The influence of sensory potentials on transcranial magnetic stimulation–Electroencephalography recordings.* Clinical Neurophysiology, 2022. **140**: p. 98-109.
53. Poorganji, M., et al., *Differentiating Transcranial Magnetic Stimulation Cortical and Auditory Responses via Single Pulse and Paired Pulse protocols: A TMS-EEG study.* Clinical Neurophysiology, 2021.
54. Raichle, M.E., et al., *A default mode of brain function.* Proceedings of the National Academy of Sciences, 2001. **98**(2): p. 676-682.
55. Machetanz, J., et al., *Magnetically induced muscle contraction is caused by motor nerve stimulation and not by direct muscle activation.* Muscle & Nerve: Official Journal of the American Association of Electrodiagnostic Medicine, 1994. **17**(10): p. 1170-1175.
56. Miller, L.E., M.R. Longo, and A.P. Saygin, *Tool use modulates somatosensory cortical processing in humans.* Journal of cognitive neuroscience, 2019. **31**(12): p. 1782-1795.
57. Restuccia, D., et al., *Modality-related scalp responses after electrical stimulation of cutaneous and muscular upper limb afferents in humans.* Muscle & Nerve: Official Journal of the American Association of Electrodiagnostic Medicine, 2002. **26**(1): p. 44-54.
58. Buchner, H., et al., *Source analysis of median nerve and finger stimulated somatosensory evoked potentials: multichannel simultaneous recording of electric and magnetic fields combined with 3D-MR tomography.* Brain topography, 1994. **6**(4): p. 299-310.